SHMS Heavy Gas Cherenkov (HGC) Detector – Winter 2018 Update

Ryan Ambrose & Garth Huber

March 1, 2018

Introduction

This update is concerned with quantifying the discrepancy in the number of photoelectrons observed in experimental data compared with the GEANT4 simulations. The calibration of the HGC is considered complete with good gain matching demonstrated. Additionally the efficiency calculation is working as intended.

Data used are from run 1583, a detector commissioning run in the winter of 2017. The configuration for this run is: carbon 0.5% target, 10 μA current, 2.2 GeV momentum, and CO_2 in the HGC at 1 atm. The optical configuration for this run was unique as well, the bottom two PMTs (1 & 2) had the optical coupling grease removed while the top two (3 & 4) did not. The only other runs analyzed are the KPP run 488 in the mirror plane comparision section and run 1911 in the efficiency section.

Gain Matching

After the detector commissioning run 488 performed in the spring of 2017, it was observed that the PMTs in the HGC had poor gain matching. For the recent detector commissioning run 1583 in the winter of 2017 new PMT voltages were calculated using the equation

$$V_{\text{new}} = V_{\text{old}} \left(\frac{\text{SPE Charge}_{\text{new}}}{\text{SPE Charge}_{\text{old}}} \right)^{\frac{1}{n}}$$

where n is a PMT dependent parameter: 10.72, 10.86, 10.57, and 8.54 for each PMT respectively. In order to allow good resolution of the SPE peak while leaving room for a large number of photoelectrons, the SPE was chosen to be located at 6.825 pC. This gave rise to the new voltages

PMT	KPP Run 488	Run 1583
1 (LL)	2347	2251
2 (LR)	2087	2051
3 (UL)	2015	2001
4 (UR)	2158	2086

The resultant pulse integral for each voltage setting is shown in Figure 1. Important to note is how the SPE peak alignment improves, in the run 488 setting the SPE varies by approximately 3 units while for the run 1583 the peaks vary by a fraction of a unit. Therefore, the HGC PMTs are very well gain matched which has implications on the calibration, making the constants between PMTs very similar.

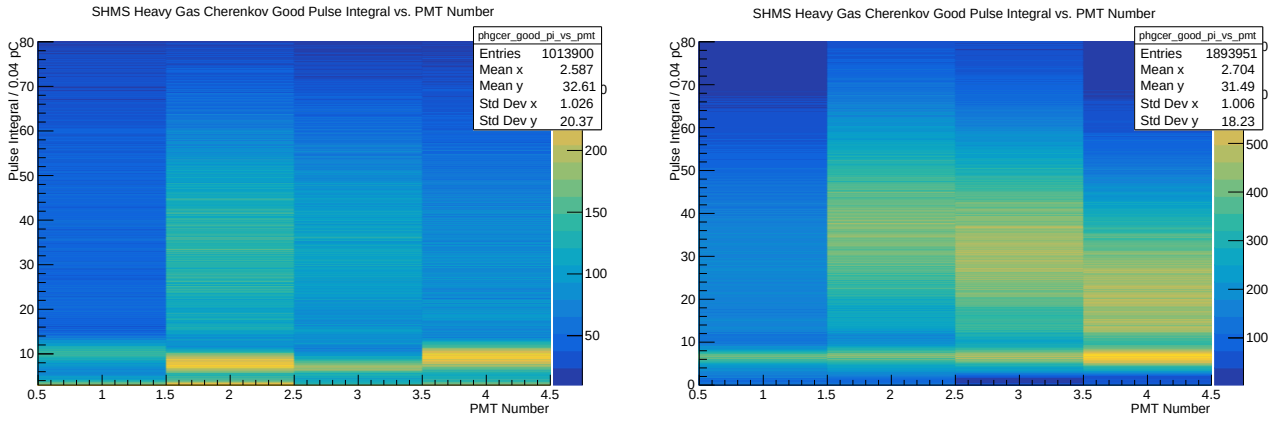

Figure 1: Comparison of gain matching between run 488 (left) and 1583 (right). Difference in voltages are shown on above table. Note that 488 Pulse Integral axis starts at 5 instead of 0 to avoid large number of counts at low pC throwing off the color scaling.

Calibration

The calibration performed on run 1583 is identical in procedure as that done for the KPP data. The only change was increasing the bin number to reduce the uncertainty in the Gaussian fit procedure. This procedure is able to clearly isolate the first, second, and third photoelectron peak as shown in Figure 2. The calibration constant is taken to be the location of the SPE peak, and the validity of the calibration is measured by aligning the photoelectron peaks with the calibrated NPE scale.

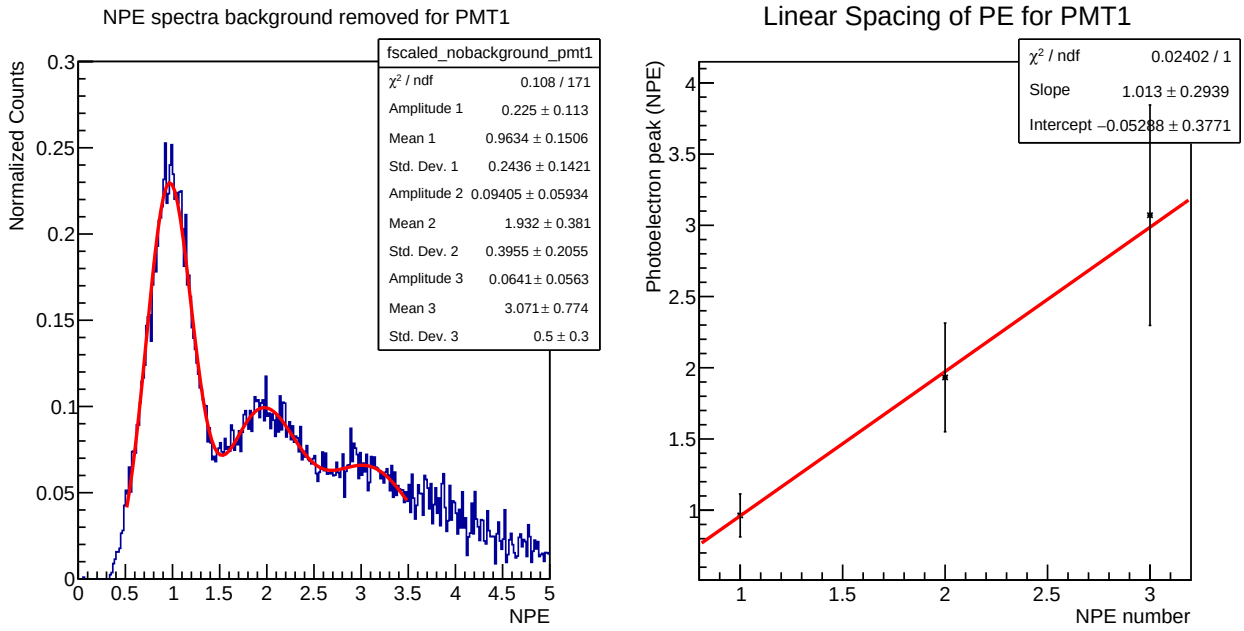

Figure 2: Results of calibrating PMT 1 (lower left) in the HGC. Left plot shows the isolated photoelectron peaks and their fitting with a sum of Gaussians. The right plot relates each peak with its mean, showing they are linearly spaced as expected.

The calibration constants for the HGC for run 1583 are shown in the table below. Because of the accurate gain matching, the constants are very similar, meaning each PMT has a similar response to incident Cherenkov light.

PMT	Calibration Constant
1	1/6.587
2	1/6.612
3	1/6.462
4	1/6.414

Efficiency

Identical to the calibration, the same procedure is used to determine the efficiency of the HGC for run 1583 as for KPP data. A cut is placed on the calibrated NPE spectra to separate electrons from pions. The percentage of electrons correctly selected is reported as electron efficiency, and the percentage of pions incorrectly identified as electrons is reported as pion leakage. This procedure is shown in Figure 3. Note that run 1911 was used instead of run 1583. This is because run 1583 had a central momentum of 2.2 GeV which is too small to produce an appreciable number of pions. This procedure can also be applied per PMT to obtain individual electron efficiency and pion leakage. The results for run 1911 with a cut at several NPE are shown on the table below. The left value is the electron efficiency and the right is the pion leakage.

NPE Cut	PMT 1	PMT 2	PMT 3	PMT 4	Full HGC
0.5	99.92% 1:14	99.99% 1:22	99.99% 1:94	99.95% 1:95	99.97% 1:41
1.0	98.34% 1:17	99.80% 1:26	99.83% 1:112	99.93% 1:112	99.73% 1:49
1.5	95.69% 1:22	99.49% 1:32	99.67% 1:148	99.89% 1:179	99.35% 1:64
2.0	93.72% 1:28	99.13% 1:37	99.54% 1:161	99.82% 1:203	99.02% 1:75

While the electron efficiency from PMT 1 seems to be significantly worse, this can be attributed to the focal plane particle dispersion. For this run mirror quadrant 1 received almost no light, and in fact PMT 1's greatest signal was from mirror quadrant 2 leading to very poor statistics. This distribution is shown in Figure 4 where one can clearly see quadrant 1 (positive x and y) receives almost no signal. Naturally, this effect will propagate to the full HGC efficiency as well.

For run 1911, the HGC was filled with C_4F_8O to 1 atm making it difficult to compare to run 1583 or run 488 since the number of photoelectrons observed is so dramatically different. However it is instructive to compare between KPP data and a more recent run to see the effect that removing the optical grease from PMT 1 and 2 had on efficiency. Therefore, the electron efficiency between run 1583 and run 488 was compared where the most significant difference is the change in beam energy (2.2 GeV for 1583 and 6.4 GeV for run 488). However, the electron efficiency should be nearly identical between these two settings and so it is assumed to be an apt comparison. The results are shown in the table below for a NPE cut at 2.0

PMT	Run 488	Run 1583	Improvement
1	85.90%	86.78%	0.88%
2	91.95%	94.49%	2.54%
3	90.87%	90.63%	-0.24%
4	88.18%	88.20%	-0.02%
Full HGC	89.72%	91.52%	1.80%

where a marked increase in efficiency is seen in PMT 1 and 2. This provides further evidence that the optical configuration of the HGC plays a role in the lower than expected NPE count in the HGC.

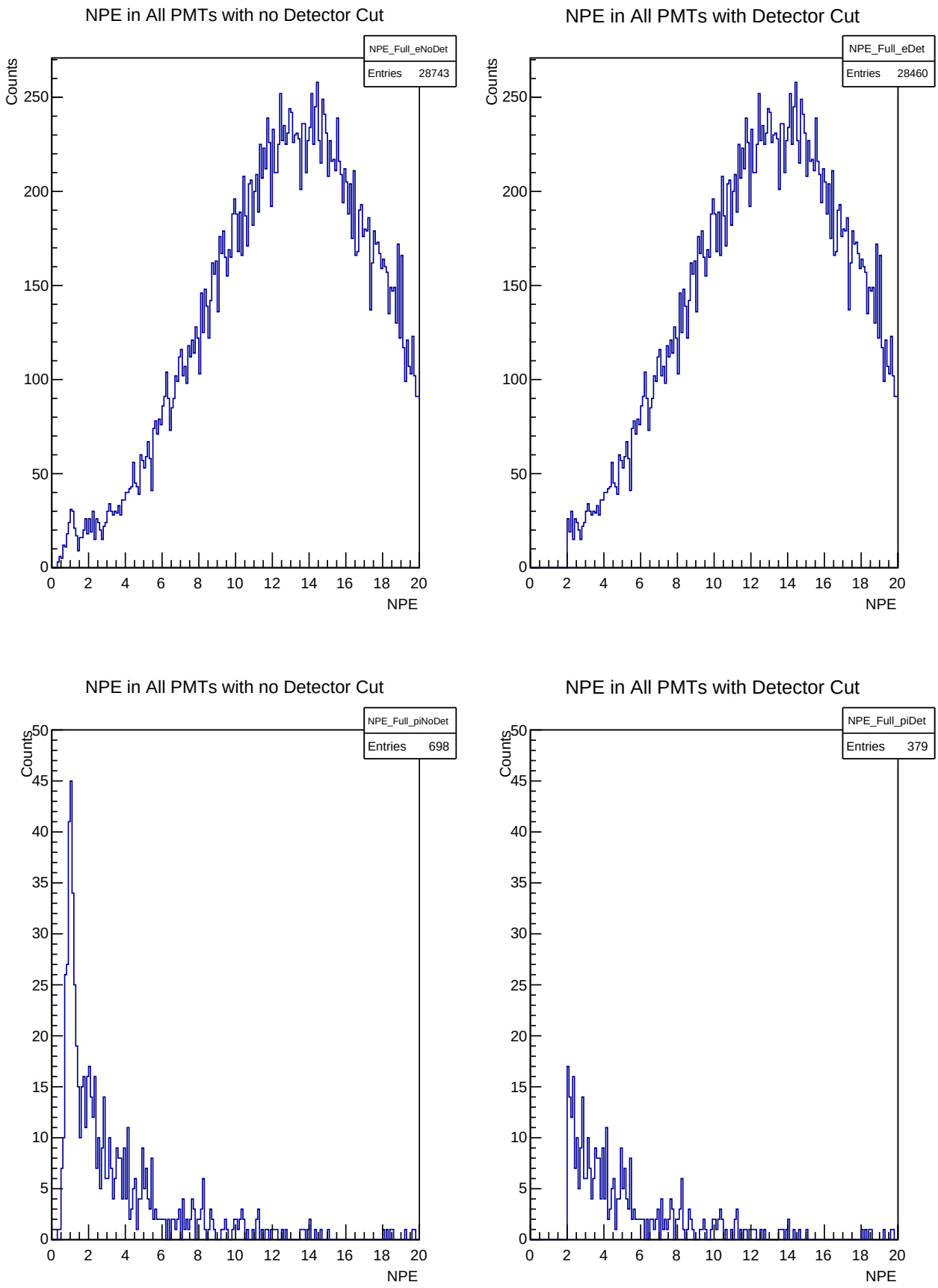

Figure 3: Results of efficiency calculation for HGC in run 1911 with a NPE cut at 2.0 NPE. This run was chosen as run 1583 has a central momentum of 2.2 GeV, too small to produce an appreciable number of pions. The top two plot show the electron efficiency where the left is the spectrum before the cut and the right is after the NPE cut is applied. The lower two plots are the same quantities for the pion.

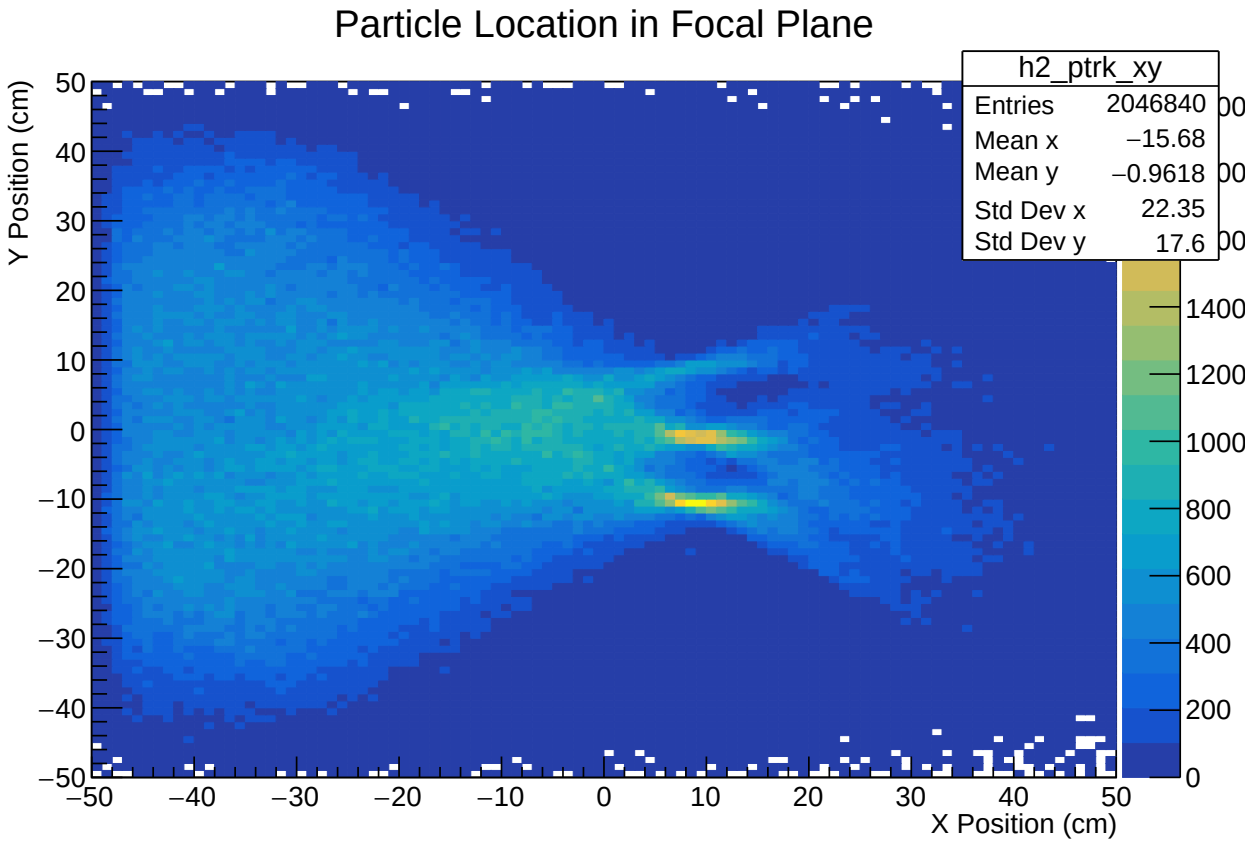

Figure 4: X-Y distribution in drift chamber focal plane of electrons. Note how few events are recorded in mirror quadrant 1 (positive x and y).

Comparison of PMT vs Quadrants

One newly investigated parameter is the individual response of each PMT to each mirror quadrant, giving rise to a 4 x 4 grid of histograms. This requires similar cuts on experimental and simulated data.

To get clean experimental data, a timing cut was applied (-30.0 ns < goodAdcTdcDiffTime < -17.0 ns) along with a particle ID cut selecting electrons. To determine which quadrant the light is coming from, the particle is projected from the focal plane position via the equation

$$y_{\mathrm{HGC}} = y_{\mathrm{DC}} + x'_{\mathrm{DC}} * z_{\mathrm{HGC}} \quad (1)$$

$$x_{\mathrm{HGC}} = x_{\mathrm{DC}} + y'_{\mathrm{DC}} * z_{\mathrm{HGC}} \quad (2)$$

into the HGC mirror plane (located at $z_{\mathrm{HGC}} = 156.27$ cm) where appropriate mirror quadrants cuts are applied according to their interleaving.

Simulated data doesn't require any "cleaning up" and instead electrons are simulated using the same running conditions. These conditions are: 2.2 GeV central momentum electrons entering the HGC filled with CO_2 at a pressure of 1.0 atm. Additionally, only PMT 3 & 4 have a layer of optical grease on them to better represent run 1583. The quadrants are selected in an identical manner as the experimental data. The position of the electrons in the focal plane is an input parameter for the simulation. This position is taken from the drift chamber information in the experimental data, so that the trajectory profile is identical between experiment and Monte Carlo.

A comparison of the experimental and simulated data for individual PMT response to each mirror quadrant is shown in Figure 5. Rows index each PMT and columns index each mirror quadrant. Blue histograms are simulated data and black are experimental data. The important comparison between the data sets is the value of mean NPE.

For the first comparison, PMT 1 & 2 have excellent agreement for quadrants 1 & 2. For quadrants 3 & 4, there is apparently a discrepancy with the anticipated mirror dispersion. This is shown by PMT 1's signal from mirror 3 and PMT 2's signal from mirror 4. Mirror 3 is dispersing more light than expected since PMT 1, 2 & 4 all observe a larger signal than expected. Conversely, mirror 4 is dispersing less light than expected since PMT 1, 2 & 3 all observe a smaller signal. The cause of this is being investigated, and may be due to slight mirror misalignment as both mirror 3 & 4 hang from the top of the HGC, however there is very little room for misalignment to occur. PMT 3 and PMT 4 are observing less light than expected from the simulation by examining the plots observing their own mirror. This is possibly due to slight mirror misalignment as well, or may be due to inaccuracies in the grease parameters in the simulation. Examining the signals in PMT 3 & 4 from mirrors 1 & 2, there is excellent agreement.

Another prominent difference between the two spectra are the large difference in counts. However it is believed that this is not an appropriate parameter for comparison. In the experiment, cuts must be performed on PMT specific leaves giving an inherent loop over all 4 PMTs for each event. For the simulation, we are able to write the PMT information directly to a histogram. Therefore there is this difference in multiplicity between the two histograms meaning the number of counts does not convey any useful information.

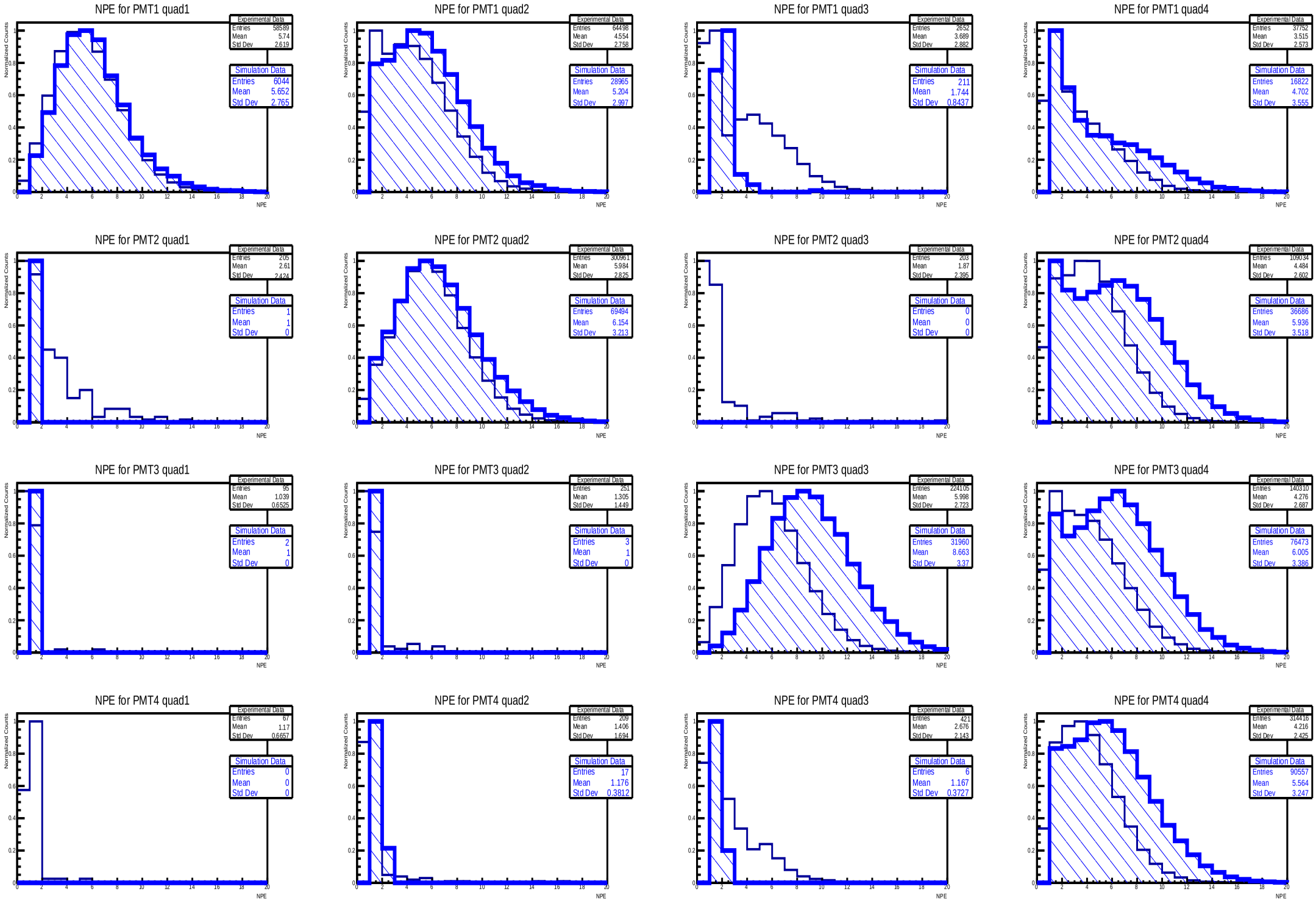

Figure 5: Description in text.

Photoelectrons in HGC Mirror Plane

Since the lower number of observed photoelectrons may have a dependence on the mirror quadrant, the light received in terms of the x-y coordinate of the HGC mirror plane was investigated. The same run 1583 was used, as well as the KPP run 488 to determine if any trends existed or are emergent. To generate the plots a TH3F histogram is produced and filled with particle location in the HGC according to Equation 1 and the sum of the number of photoelectrons from each PMT. This histogram is then projected to produce a TH2F profile where the z-axis is converted into a color map of average NPE for the x-y bin. This is shown in Figure 6.

To verify the localized regions of lower NPE are not a binning issue, Figure 7 shows specific ranges of NPE from the TH3F histogram before any averaging. This reveals that some regions are biased towards a lower NPE count. To verify this is not a recent phenomena, run 488 from the 2017 spring KPP commissioning was similarly analyzed in Figure 8 and Figure 9. In these figures the regions are identical, suggesting they are related to the HGC optical configuration. This is the likely conclusion since each run had a different focal plane trajectory profile, and an issue with mirror alignment would cause the full quadrant to have a lower count, not just a localized region.

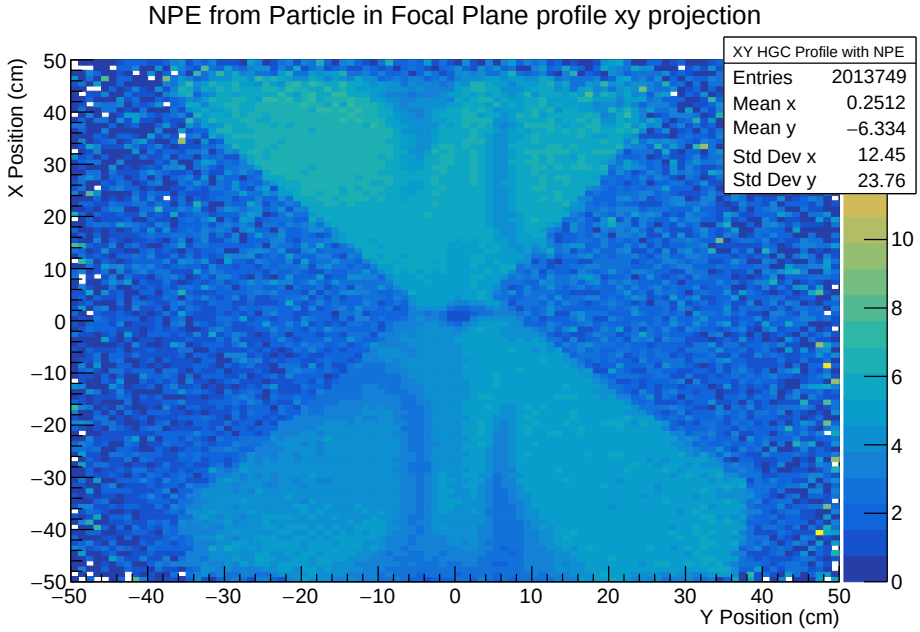

Figure 6: Number of photoelectrons received in the HGC across the mirror plane. Color axis refers to the number of photoelelectrons. Run 1583.

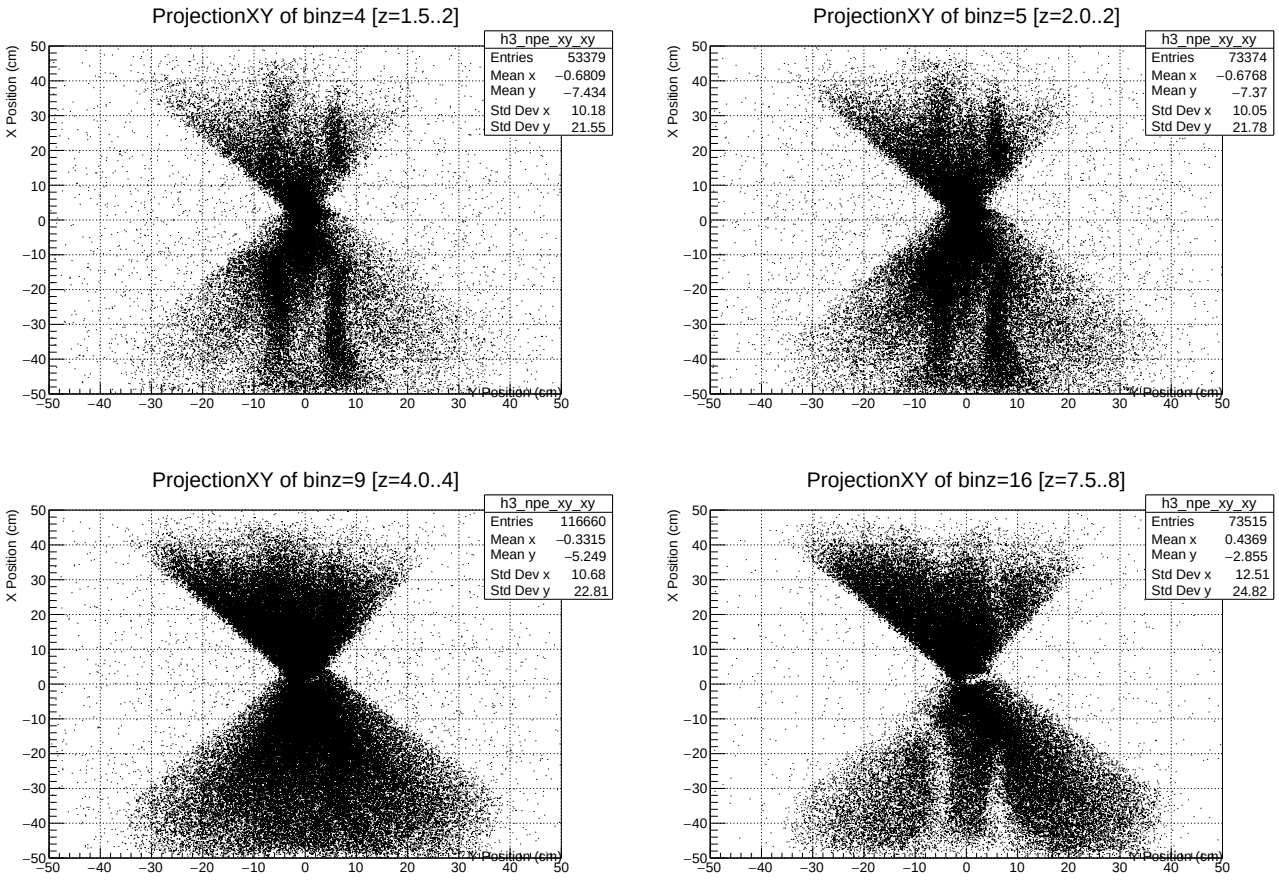

Figure 7: Number of photoelectrons received in the HGC across mirror plane separated into specific ranges of NPE. Ranges starting top left and following clockwise: 1.5 - 2.0, 2.0 - 2.5, 7.5 - 8.0, 4.0 - 4.5. Run 1583.

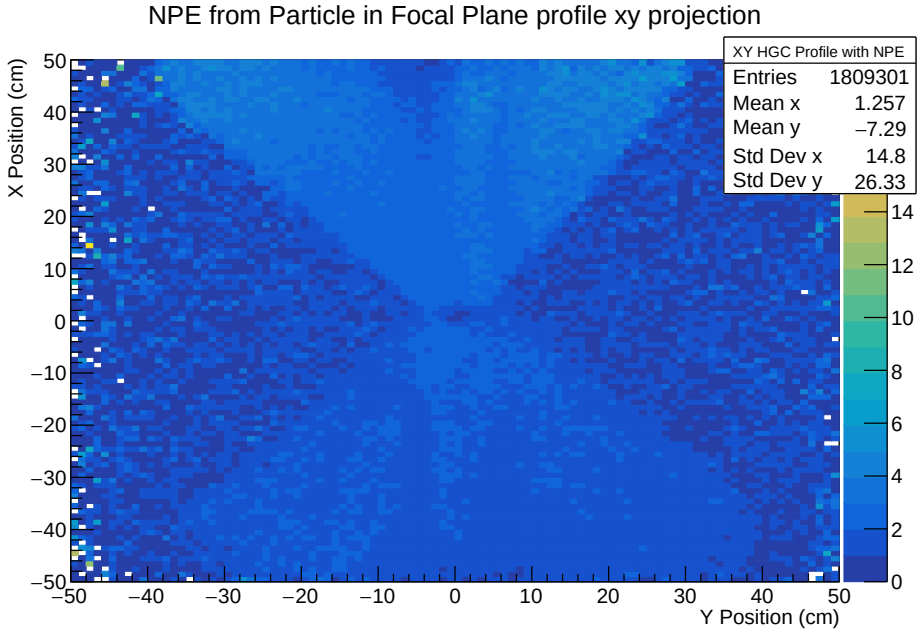

Figure 8: Number of photoelectrons received in the HGC across the mirror plane. Color axis refers to the number of photoelelectrons. Run 488.

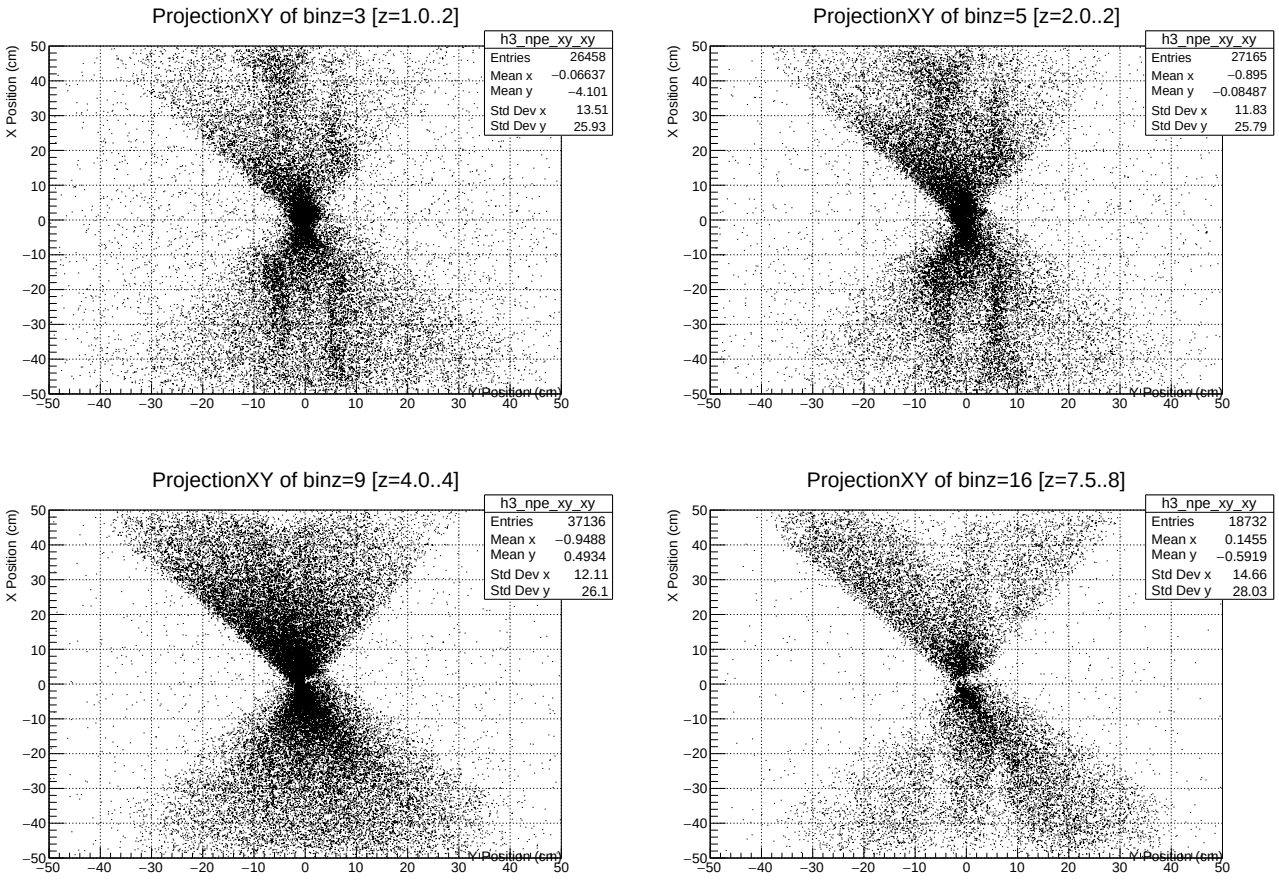

Figure 9: Number of photoelectrons received in the HGC across mirror plane separated into specific ranges of NPE. Ranges starting top left and following clockwise: 1.0 - 2.0, 2.0 - 2.5, 7.5 - 8.0, 4.0 - 4.5. Run 488.

New Optical Configuration

To improve the performance of the HGC, a new choice for the optical configuration has been explored. After researching each component and testing them in simulation, it was determined that a solution is to replace the current combination of grease, adapter, and RTV coupling to the PMT (shown in Figure 10) with simply a ring lined with aluminum. The ring will hold the PMT approximately 2 mm from the window surface with the aluminum serving to reflect divergent light back towards the PMT cathode. An top view of this new optical object is given in Figure 11 with a side view in Figure 12. An alternate view of how the ring will fit with the PMT and nu-metal shield is provided in Figure 13. In the simulation it was found that most losses occur traversing the various optical media, and passing through the various thresholds. By replacing this with a simpler single interface (window to air) an increase to NPE is expected. The results of simulation, shown in a similar format as Figure 5, are displayed in Figure 14. While these simulation results should be considered an optimistic projection of HGC performance, particularly for PMT 3 and 4 where in Figure 5 they overestimate by 30% and 24% respectively, this result is suggesting an improvement to the signal should be anticipated. Average number of photoelectrons detected in run 1583 compared to the average in the new simulation, along with the percentage improvement, are shown in the table below.

PMT	Current NPE	Simulated NPE	Improvement
1	4.42	17.17	388%
2	5.31	19.33	364%
3	5.31	17.56	331%
4	4.24	15.25	360%
Full HGC	4.91	20.20	411%

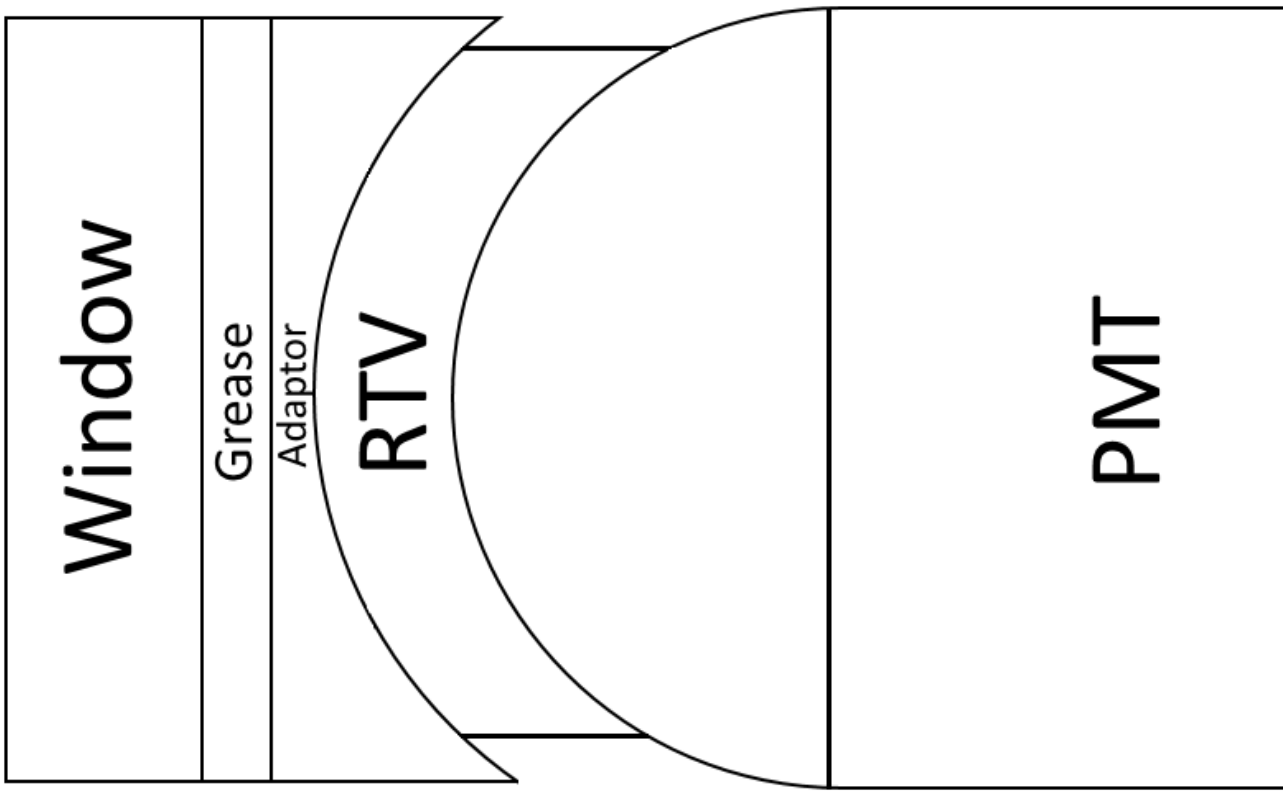

Figure 10: Depiction of old optical configuration of HGC. Note that the components are NOT to scale.

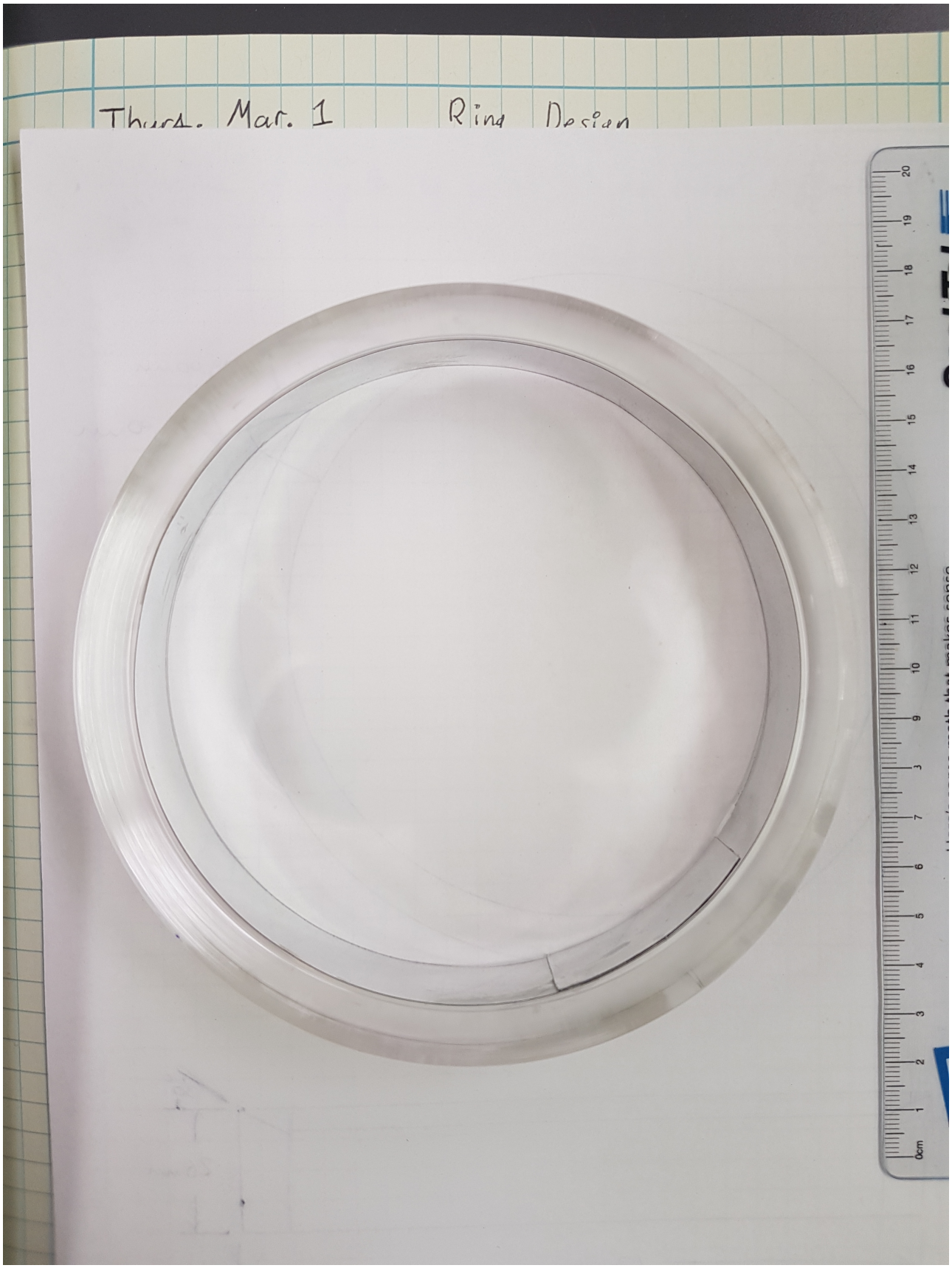

Figure 11: Top down view of new optical object. Ruler is given for scale of object.

Figure 12: Side view of new optical object. Notice that the layer of aluminum is short of beveled surface to ensure no contact is made with PMT glass.

Figure 13: View of Burle PMT in a nu-metal shield without (above) and with (below) the new ring design. Note how the strip of aluminum does not contact the PMT window surface.

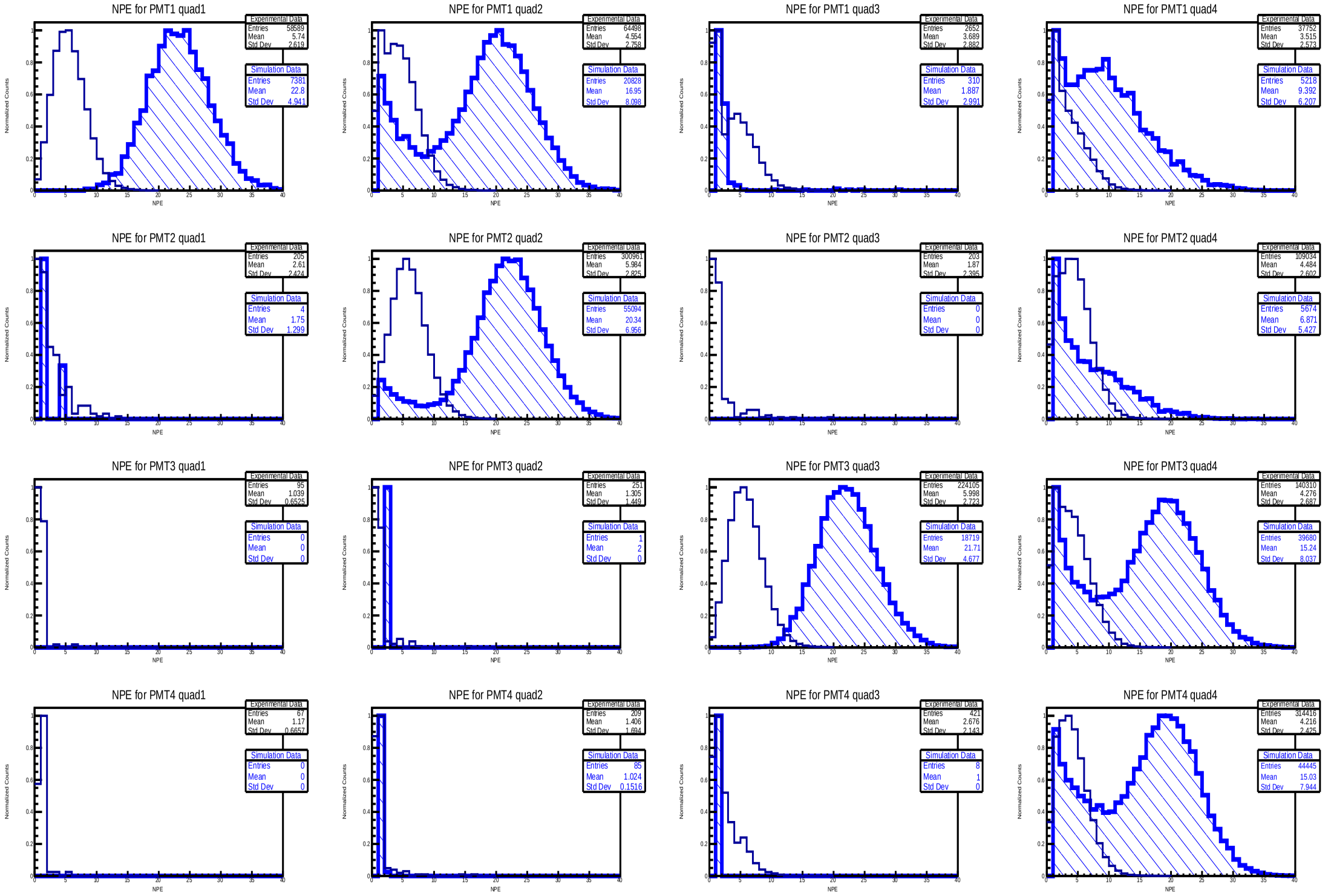

Figure 14: Description in text.